LASER & PHOTONICS REVIEWS
www.lpr-journal.org

Increasing Efficiency of Ultrafast Laser Writing Via Nonlocality of Light-Matter Interaction

Huijun Wang, Yuhao Lei, Gholamreza Shayeganrad, Yuri Svirko, and Peter G. Kazansky**

In ultrafast laser writing, and light-matter interaction in general, it has been widely accepted that the higher the energy density, the stronger material changes occur, unless thermal effects are involved. Here, this belief is challenged by demonstrating that a decreased energy density—achieved through increased scanning speed and without thermal accumulation—surprisingly leads to a more significant modification of silica glass, i.e, a higher increase in the isotropic refractive index or greater birefringence of nanopore-mediated modification. This counterintuitive phenomenon is attributed to the nonlocality of light-matter interaction at tight focusing, where the intensity gradient of the light beam and associated diffusion of charge carriers play a critical role in increasing material modification. A tenfold increase in the writing speed of the polarization multiplexed data storage with the potential to achieve MB s^{-1} using high transmission nanopore-based modification.

1. Introduction

Advances in laser technology, such as chirped-pulse amplification (CPA),[1,2] have made it possible to generate intense light pulses in the femtosecond regime enabling light-matter interaction with rapid and precise deposition of energy in transparent materials. In the nonlinear regime, light produces free electrons in bulk of transparent medium via multiphoton and/or tunnelling,[3,4] and avalanche ionization.[5–7] Transferring energy of these electrons to the lattice causes irreversible material modification,[8–10] which is often referred to as ultrafast laser writing. Depending on irradiation conditions, the permanent material modification can result in positive refractive index changes (type 1),[11–13] form birefringence produced by self-assembled nanogratings (type 2)[14–17] or flattened nanopores (type X),[18] void structures (type 3),[19,20] and phase transitions from the crystalline to the amorphous state [21,22] or vice versa.[23,24] Despite the fact that the effect of laser writing parameters including wavelength,[25] pulse duration,[26] repetition rate,[27] and pulse/energy density[28,29] on the strength of material modification has been thoroughly investigated, the underlying physical mechanisms have not been fully understood. As a result, efficient energy deposition for a wide range of applications of ultrafast laser writing in transparent materials that span from integrated optics[30,31] and microfluidics[32] to polarization beam shaping and optical data storage[33] still remains a key challenge. In particular, the inherent reduction of energy density with the increase in scan speed results in reduced strength of material modification and overall throughput. It should be mentioned that an increase of positive index change with an increase in the scanning speed was observed at high repetition rates of tens of MHz and high pulse energies and was explained by the mechanism of a fictive temperature rise when it is not limited by the thermal diffusion.[34] Increasing the write speed is also critical, for the development of multidimensional data storage with polarization multiplexing in glass. This is a world-first technology designed and built from the media up to address humanity's need for a long-term, sustainable storage solutions.[35] Ultralow loss ultrafast laser nanostructuring (type X), which has potential to allow thousands of layers to be recorded, is of particular interest for this application and next generation of cold storage in data centers.[35,36] This advantage of nanopore-mediated X-type birefringent modifications is limited by the reduced writing speed since tens of pulses are required to create this type of modification. By comparison, nanovoid-mediated lamella modifications can be created in just a few pulses[37] at the cost of lower transmission requiring more sophisticated readout technology for multilayer recording (more than hundreds of layers).

Here, we demonstrate that stronger modification can be imprinted at a lower energy density during high-speed scanning writing of voxels (volumetric pixels) in silica glass. Surprisingly, the positive refractive index change and birefringence produced by nanopore formation are non-monotonous functions of the scan speed, with the maximum shifting toward the higher scan speed with fewer pulses. Due to the relatively low temperature involved in the laser writing process to achieve ultralow loss

H. Wang, Y. Lei, G. Shayeganrad, P. G. Kazansky
Optoelectronics Research Centre
University of Southampton
Southampton SO17 1BJ, UK
E-mail: Huijun.Wang@soton.ac.uk; pgk@soton.ac.uk
Y. Svirko
Center for Photonics Sciences
University of Eastern Finland
7 Yliopistokatu, Joensuu 80100, Finland

DOI: 10.1002/lpor.202301143

modifications, the fictive temperature mechanism required temperatures more than a thousand degrees in fused silica is not applicable. We interpret the observed phenomenon in terms of the nonlocal light-matter interaction, which leads to the enhancement of the material modification due to charge carrier separation in the tightly focused light beam with high intensity gradient. This conclusion is of fundamental importance and has implications far beyond just ultrafast laser writing in transparent materials, but to light applications for material modification or processing.[38,39] The phenomenon is used for type X, ultralow loss ultrafast laser nanostructuring and demonstration of polarization multiplexed optical data storage with increased writing speed at high pulse repetition rate with the thermal accumulation reduced by pulse energy modulation (PEM). A digital document is optically encrypted into 42 layers in silica glass with the writing speed of 72 kB s^{-1} and 100% readout accuracy.

2. Results and Discussion

Birefringent voxels with high transmittance produced by nanopore formation were written at different scanning speeds (v_s from 2 mm s^{-1} to 50 mm s^{-1}) and five different numbers of pulses (N_p from 15 to 35) while keeping repetition rate at 1 MHz and other parameters the same (**Figure 1a**). During the writing of the voxels, the laser beam remained stationary, and the translation stages moved at varying speeds. Precise control over the pulse number for each voxel was achieved using a gate signal from a signal generator to the pulse-picker within the laser. For example, to achieve a pulse number of 30 at a 200 kHz repetition rate, a 150 µs gate signal was used, equivalent to 30 × 5 µs. The slow axis orientation of birefringent voxel was perpendicular to the polarization azimuth of a laser writing beam. Contrary to intuition, the retardance of birefringent modification first increases and then drops as the scanning speed increases (Figure 1b). Furthermore, the peak value shifts to lower scanning speed as the pulse number increases, i.e., the maximum retardance appears at scanning speeds of 25 mm s^{-1}, 30 mm s^{-1}, 35 mm s^{-1}, and 40 mm s^{-1} for pulse numbers of 35, 30, 25, and 20, respectively. The diameter of each voxel was estimated from the birefringence image as full width half maximum of retardance distribution fitted with a Gaussian function (Section 1 in Supporting Information). It is clearly illustrated that the modification size along scanning direction increases with scan speed due to the relative position shift of laser beam (Figure 1c). In addition, for $N_p = 30$ and $N_p = 20$, the position shift of all pulses is larger than the modification size for speeds higher than 30 mm s^{-1} and 40 mm s^{-1}, respectively, indicating that the retardance of birefringent voxels starts to decrease when the position shift is greater than the modification size:

$$l_{shift} = N_p \cdot v_s \cdot \Delta t > D_{mod} \quad (1)$$

where $\Delta t = 1/RR$ is the time interval between pulses and D_{mod} is the diameter of modification. Furthermore, no effect of voxel length and lateral separation was observed in the relationship between retardance increase and scanning speed (Section 2 in Supporting Information). In addition, the refractive index changes indicate a non-monotonous trend of birefringence, consistent with the findings from the retardance measurements (Section 3 in Supporting Information). It should be noted that the retardance measurements shown in Figure 1b and Figure S4 (Supporting Information) represent averages obtained from eight different polarizations of the writing laser beam. The polarization dependent modification strength is also affected by the scanning speed (Figure 1d,e). At relatively low scan speeds, the maximum retardance of birefringent modification occurs when the polarization direction of the writing laser beam is parallel to the scan direction (slow axis azimuth close to 90 degree). We propose that this phenomenon can be attributed to the nonlinear currents,[40–42] which are driven by the concentration gradient and directed along the polarization of the light. However, when the scanning speed is higher than 25 mm s^{-1}, the relationship between modification strength and polarization is reversed. In other words, the modification is strongest for the polarization perpendicular to the scanning direction. This is due to the elongation of voxels along scan direction when the slow axis is oriented at 0 degree, resulting in larger modification size and shift in maximum retardance to higher speeds.

The dependence of optical path difference (OPD) due to the isotropic refractive index increase and the retardance dependence for nanogratings-based birefringent modification on scanning speed were also investigated. The voxel writing of type 1 modification has a similar tendency to type X, that is, the OPD first increases and then decreases with scan speed (**Figure 2a**). Compared to type X modifications, the maximum OPD of type 1 occurs at a higher scanning speed for the same pulse number, satisfying Equation (1). This is attributed to the larger modification size of type 1 voxels (Section 4 in Supporting Information). On the other hand, the writing pulse energy is larger for the nanogratings regime of modification than that required for the formation of anisotropic nanopores. A significant increase in retardance (up to 2 times) was observed at a pulse energy of ≤ 200 nJ with a number of pulses of 30 (Figure 2b), in which all modifications were of type X. When the energy increased to 205 nJ, the transition from modification of the nanograting type 2 to the nanopore type X was observed with a change in the scanning speed. The nanogratings were generated at $v_s \leq 15$ mm s^{-1} where the retardance was almost unchanged, while flattened nanopores were formed for $v_s > 15$ mm s^{-1}, after which the retardance first increased and then decreased. Moreover, for pulse energy ≥ 200 nJ, only type 2 modification was imprinted and there was no increase in retardance with scan speed, which was similar to the trend for single nanolamella-like structures (Section 5 in Supporting Information). The mechanism of anisotropic nanopores generation in silica glass can be explained by two processes: formation of randomly distributed nanopores and flattening of the nanopores perpendicular to the laser beam polarization.[18,43] Additionally, the retardance of type X voxel written in a nanopores glass sample was not changing with scanning speeds, indicating that the extraordinary increasing phenomenon should be associated with the formation rather than the reshaping of the nanopores (Section 6 in Supporting Information).

The observed increase in the strength of both positive refractive index change and nanopores-based modification as well as constant strength of modification for nanograting-type with increasing scanning speed is puzzling. Indeed, at the same number of pulses, the higher the scan speed, the larger the irradiated area and the lower the deposited energy density. The puzzle can

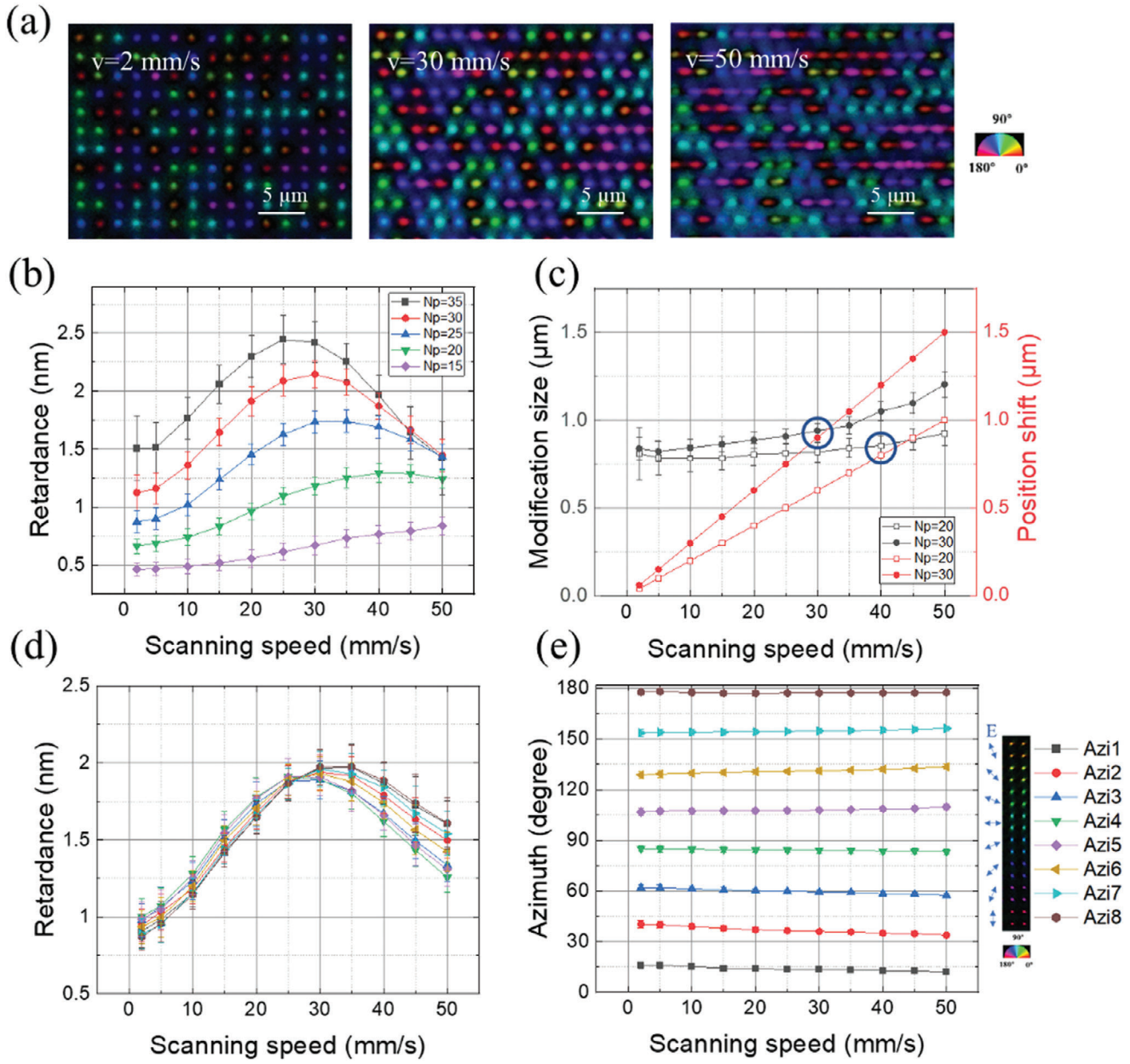

Figure 1. Type X modification as a function of scanning speed. a) Birefringent images of voxels written at 3 different writing speeds and $N_p = 30$. Lateral voxel separation was 2 μm. Pseudo-colors (inset) indicate the local orientation of the slow axis. b) Retardance of the birefringent voxels versus scanning speed for five different pulse numbers. c) Dependence of modification size along scanning direction and position shift of all pulses on scanning speed for pulse numbers 20 and 30. d) Retardance and e) slow axis azimuth dependence on scanning speed for eight different polarizations and $N_p = 30$. The retardance is maximum in blue-circled regions in (c). Writing conditions: 1 MHz repetition rate, 300 fs pulse duration, 190 nJ pulse energy, 0.3 *NA* lens.

probably be solved if one assumes that the mechanism of material modification is nonlocal, i.e., the modification depends not only on the fluence or density of the photoexcited carriers, but also on its gradient. This implies that the diffusion of the carriers created by photo- and avalanche ionization of the silica atoms should play an important role in the modification process.

To clarify the mechanism of the material modification we may distinguish processes involved by their characteristic times. In the sub-picosecond time frame, free carriers are generated in the irradiated volume by laser pulse with duration of $\tau = 300$ fs. The temporal evolution of the electron density n_{e0} in the silica is governed by the following equation:[5,44]

$$\frac{\partial n_{e0}}{\partial t} = \sigma_n I^n + \alpha_{av} n_{e0} I - \frac{n_{e0}}{\tau_r} \tag{2}$$

where $I = I(r,t)$ is the intensity of the laser pulse, σ_n is n-photon absorption cross section, α_{av} determines the avalanche ionization rate, and $\tau_r \approx 150$ fs is the electron trapping time.[45] The trapping time is associated with the formation of self-tapped excitons

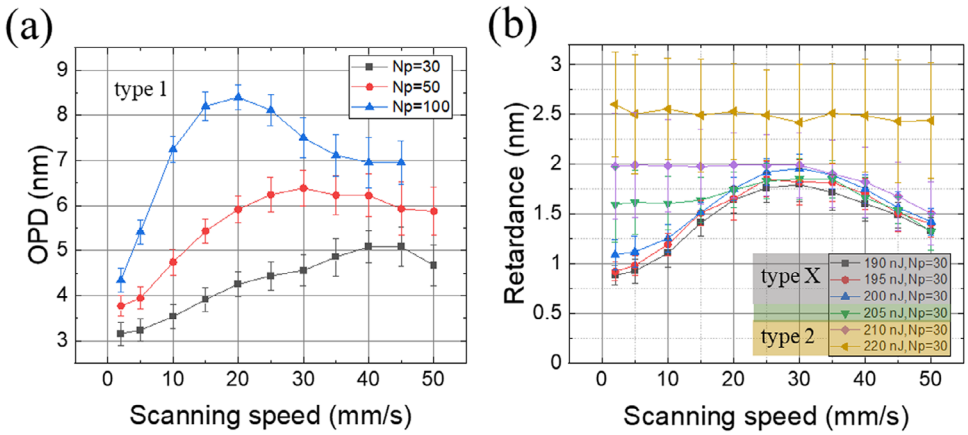

Figure 2. Influence of scanning speed on different types of modification. a) Dependence of optical path difference (OPD) of refractive index increase on scanning speed for three different pulse numbers. The pulse energy is 170 nJ, repetition rate is 1 MHz, pulse duration is 190 fs and numerical aperture of the lens is 0.3. b) Retardance of birefringent voxels dependent on scanning speed with different pulse energies. The repetition rate is 1 MHz and the pulse duration is 300 fs.

in silica glass, which really concerns exciton, i.e., simultaneous trapping of hole and electron.[46] The ionization of SiO_2 atoms gives rise to the fast increase of the electron density, however the number of electrons generated in the center of the beam is much higher than that at the periphery. The gradient of the concentration initiates the diffusion current, i.e., the free electrons move toward the beam periphery leaving behind positively charged holes (ionized silica atoms, O^-) (**Figure** 3a,left).

The electrons are able to move during electron-phonon relaxation time $\tau_{eph} \approx 1$ ps.[47] In this timescale, the diffusion current, which is governed by the concentration gradient, creates an electric field (E_c) directed from the center to periphery of the beam (Figure 3a,middle). Although the electron dynamics is terminated at the timescale of less than 1 ps, the influence of the previous pulse will not disappear. The diffusion current of electrons creates the separation of charges because electrons are trapped at the boundaries of irradiated region. Then a positively charged center and negatively charged boundaries are formed, affecting the interactions between subsequent pulses and material. Free electrons are trapped by defects in the glass structure, particularly shallow traps produced by glass disorder. On the other hand, the holes remaining in the irradiated region are self-trapped. The lifetime of self-trapped holes (STH), especially with an excitation energy of around 1 eV, is relatively long.[48] The lifetime of separated charges and the induced direct current (DC) field is very long because the dark conductivity of silica glass is low. In other words, when irradiated with a laser pulse, electrons are first excited and then diffuse from the center to the boundaries, producing an electric field. The second-order nonlinearity created by this electric field is responsible for the second harmonic generation signal upon the irradiation of subsequent intense femtosecond laser pulses.

The second harmonic (SH) intensity distribution revealed a two-lobe pattern aligned with the pump polarization azimuth for linear polarization and a donut-shaped pattern for circular polarization (Figure 3b). The axisymmetric SH intensity profiles are in good agreement with the radial distribution of the space charge field. Moreover, due to angular momentum conservation, the SH generated by the pump with the circular polarization is indeed a vortex SH beam.[49–51] The spatio-temporal evolution of the electron density n_e and generated DC field E_c is governed by the following equations:

$$\frac{\partial n_e}{\partial t} = -\nabla\left(-\mu_e n_e E_c - D_e \nabla n_e\right) \tag{3}$$

$$\varepsilon_0 \varepsilon \nabla E_c = e\left(n_h - n_e\right) \tag{4}$$

where μ_e and D_e are the mobility and diffusion coefficient of electrons in silica, respectively, n_h is holes density, ε_0 is the vacuum permittivity, and ε is the silica dielectric constant. Since Equations (3) and (4) describe the behavior of the system after the excitation pulse, it should be solved using initial conditions $n_e(0,r) = n_{e0}(t = \tau, r)$, $E_c(0,r) = 0$. Since the holes do not move in this time scale, their spatial distribution in the irradiated volume does not depend on time and is determined by the initial electron density, i.e., $n_h(t,r) = n_{e0}(t = \tau, r)$. (Section 7 in Supporting Information).

For stationary writing of voxels, the induced electric field E_c formed by the preceding pulses impedes diffusion of electrons generated by subsequent pulses. However, under scanning writing, the center of the photoexcited region is shifted and the hindering effect of E_c is reduced, resulting in more efficient diffusion of electrons and larger density of self-trapped holes (Figure 3a,right), the clustering of which could facilitate the formation of nanopores and generate stronger modification. This idea is also supported by our recent work on ultrafast laser writing in silica glasses of different grades.[42] The numerical simulation based on Equations (3) and (4) reveals that the electric field increases with position shift and becomes saturated after 0.8 μm (Figure 3c), which is consistent with the observed increasing strength of modification in the experiment. The density of self-trapped holes, accompanied by the electric field, increases for ≈ 40% when the position of the beam center is shifted by 1 μm.

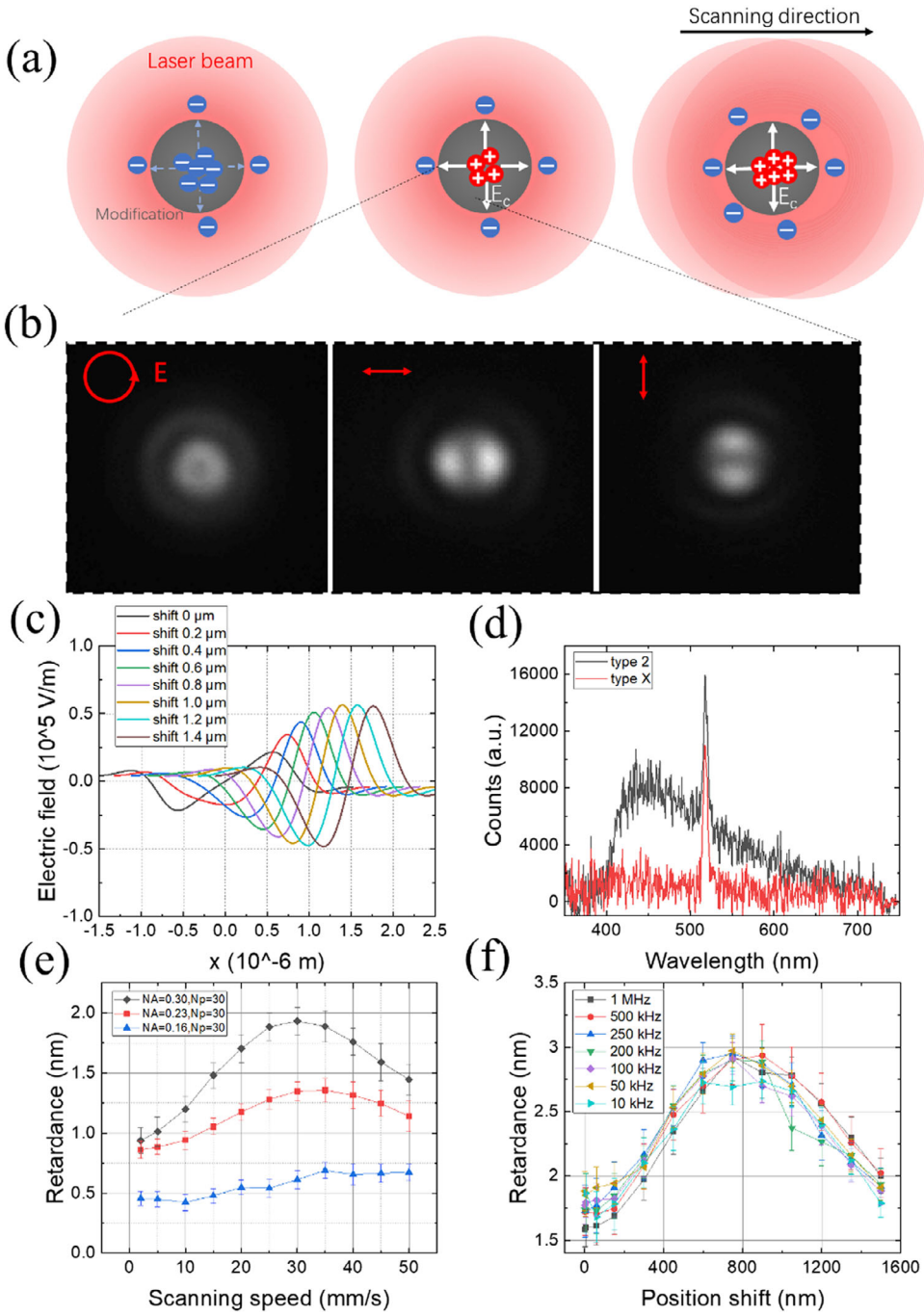

Figure 3. Material modification by ultrashort laser pulses. a) Mechanism illustration of electron concentration gradient and diffusion (left), space charges and build-up electric field (middle), and larger density of holes during scanning (right). b) Electric field induced SH patterns for different polarizations under continuous irradiation. c) Simulated electric field generated by the last (40^{th}) pulse with different position shifts. d) Spectrum of the light emission with wide spectral distribution between 350 nm and 750 nm for the conditions of both type 2 and type X at scanning speed of 1 mm s^{-1}. e) Retardance of birefringent voxels versus scanning speed with different numerical apertures. f) Retardance versus position shift with different repetition rates varying from 10 kHz to 1 MHz. Writing conditions: 1030 nm wavelength, 300 fs pulse duration, 190 nJ pulse energy, 30 pulse number, and 0.3 NA lens.

More specifically, we utilized a Matlab code to solve Equation (3) after each pulse. The initial electric field (E_c) of the first pulse was set to 0:

$$n_e\ (t) = n_e\ (t-1) + -\nabla\left(-\mu_e n_e\,(t-1)\,E_c - D_e \nabla n_e\,(t-1)\right) dt \quad (5)$$

After the diffusion of electrons, the separated electrons and holes induce an electric field E_c, which is calculated using Equation (4). This allowed us to obtain the electron density and electric field over time. For multiple pulses, in the simulation of the next pulse (n^{th}, $n \geq 2$), we used a newly generated electron

density without adding the previous n_e, that is $n_e(\Delta t(n-1), r) = n_{eo}(t = \tau, r)$ since the pulse interval is in the microsecond scale. However, the electric field is "frozen" and added to the initial condition of the next pulse: $E_c(\Delta t(n-1), r) = E_c(\Delta t(n-2) + t, r) + E_c(\Delta t(n-2), r)$, where t is the diffusion time. The simulated electron density and electric field at the final pulse (40^{th}) after diffusion time for different position shifts are shown in Figure 3c and Figure S10 (Supporting Information), respectively. The induced electric field increases with the position shift of all pulses and reaches saturation after 0.8 μm. This indicates that the density of self-trapped holes increases with position shift/scanning speed, resulting in increased birefringence. The simulation correlates well with the experimental results, with the maximum retardance occurring when the position shift is close to the modification size of ≈ 0.9 μm. After this peak, the retardance decreases due to the modification being clearly elongated in the scanning direction.

In order to prove the DC electric field generation in the irradiated volume of the silica, we also measured the second harmonic germination during writing experiments at $RR = 500$ kHz and the pulse train of $N_p = 40$ (Figure 3d) (Section 8 in Supporting Information). The SH signal was indeed observed, evidenced by the peak around 515 nm in the light emission spectrum. The estimated SH conversion efficiency is ≈ 3×10^{-9}. Assuming interaction length of 10 μm, the effective second order nonlinearity in our experiment is ≈ 2×10^{-16} m V^{-1}, and the value of electric field estimated by $\chi^{(2)}_{eff} = 3E_c\chi^{(3)}$ is 3×10^5 V m^{-1},[52] which is about an order of magnitude larger than the value in the simulation, probably due to the accumulation for all pulses in the SH measurement.

Interestingly, in the nanograting formation regime (type 2), we observed also emission band centered at 450 nm. We believe that this emission originates from blue luminescence of self-trapped excitons at 2.8 eV [53,54] rather than from plasma. On the contrary, in the regime of nanopore formation (type X), no emission at 450 nm was observed because of either luminescence quenching or a lower concentration of self-trapped excitons. In this regime, the mechanism of the material modification is different from that responsible for the nanograting formation as one can observe from the scanning speed dependence (Figure 2).

Furthermore, we found that the retardance dependence on scanning speed is similar for three different numerical apertures (Figure 3e). However, for the same pulse number, the scanning speed at which the maximum retardance emerges is slightly larger for smaller numerical aperture lens. For instance, for $N_p = 30$, maximum retardance is obtained at a scanning speed of 30 mm s^{-1} with $NA = 0.3$, while that appears at 35 mm s^{-1} with $NA = 0.16$, which can be attributed to the larger modification size with a 0.16 *NA* lens. On the other hand, the amount of increase in retardance for different *NAs* is different, that is, the retardance was increased by 105% for $NA = 0.3$, 58% for $NA = 0.23$, and 50% for $NA = 0.16$, while the intensities were almost the same, i.e., 9.3 TW cm^{-2}, 9.2 TW cm^{-2} and 7.3 TW cm^{-2}, respectively. Interestingly, more significant retardance increase can be realized by utilizing a higher numerical aperture, which confirms our conjecture about the importance of gradient and is preferable for data storage with high writing speed and data capacity.

According to Equation (1), for the same pulse number and modification size, maximum retardance appears at a higher scanning speed for a higher repetition rate. In order to further validate the impact of repetition rate on the peculiar highly transmitting birefringent voxels with increasing scanning speed, we conducted experiments under $NA = 0.3$, $N_p = 30$ and $\tau = 300$ with a pulse energy of 190 nJ. We specifically altered the repetition rates from 10 kHz to 1 MHz (Figure 3f) while keeping the scanning speed range variable to maintain a consistent pulse density/position shift of all pulses across different rates. For instance, the scanning speeds ranged from 20 μm s^{-1} to 50 mm s^{-1} for a repetition rate of 1 MHz, from 2 μm s^{-1} to 5 mm s^{-1} for 100 kHz, and from 0.2 μm s^{-1} to 0.5 mm s^{-1} for 10 kHz. Across all different repetition rates, the observed trend remained largely consistent, with the maximum retardance occurring at a position shift of ≈ 800 nm. This corresponds to ≈27 mm s^{-1} for 1 MHz, ≈2.7 mm s^{-1} for 100 kHz, or ≈0.27 mm s^{-1} for 10 kHz. This confirms that the observed increasing trend is related to the deposited energy density. In other words, a faster writing speed can be achieved by using a higher repetition rate while maintaining the maximum retardance.

Birefringent voxels were also written with increased repetition rates (RR from 1 to 5 MHz) to explore further the feasibility of high-speed writing (**Figure 4a**). The scanning speed varied from 50 mm s^{-1} to 250 mm s^{-1} to keep the same deposited energy density. X-type modification was observed at repetition rates of both 1 MHz and 2 MHz, but unexpectedly, the strength of the birefringent modification turned out to be stronger at $RR = 2$ MHz, which can possibly be explained by the accumulation of defects, for example, non-bridging oxygen hole centers.[36,55] However, when the repetition rate was increased to 3 MHz, damage emerged and the structures were completely destroyed at $RR = 4$ MHz or 5 MHz, which could be attributed to the heat accumulation. The thermal effects can be mitigated if a modification is produced with an efficient modulation of energy deposition, meaning more energy is used to modify rather than heat the material (**Figure 4b**) (Section 9 in Supporting Information). Compared with nanolamella-like structure generated via PEM,[37] multilayer data storage with 100% readout accuracy can be achieved due to high transmission of type X modifications, enabling data storage without error correction.

Data recording of 4 bits per voxel with 3 MHz and 3 bits per voxel with 5 MHz was demonstrated (Section 10 in Supporting Information). In order to test the multi-layer data recording with nanopore-based high transmission birefringent modification using high writing speed, the digital copy of an iconic book was recorded in 42 layers (**Figure 5a**). The text data were encrypted by randomly assigning numbers (from 0 to 7) to the 8 slow axis orientations and encoded by American Standard Code for Information Interchange code, where every three voxels correspond to a character. The readout accuracy was 100% for both the 1st layer and the 42nd layer (Figure 5b). Lateral voxel separation and layer separation were only 1.3 μm and 14.6 μm, respectively, using a 0.3 numerical aperture lens, corresponding to a data capacity of 735 GB per 127 mm disk and a data write speed of 72 kB s^{-1}.

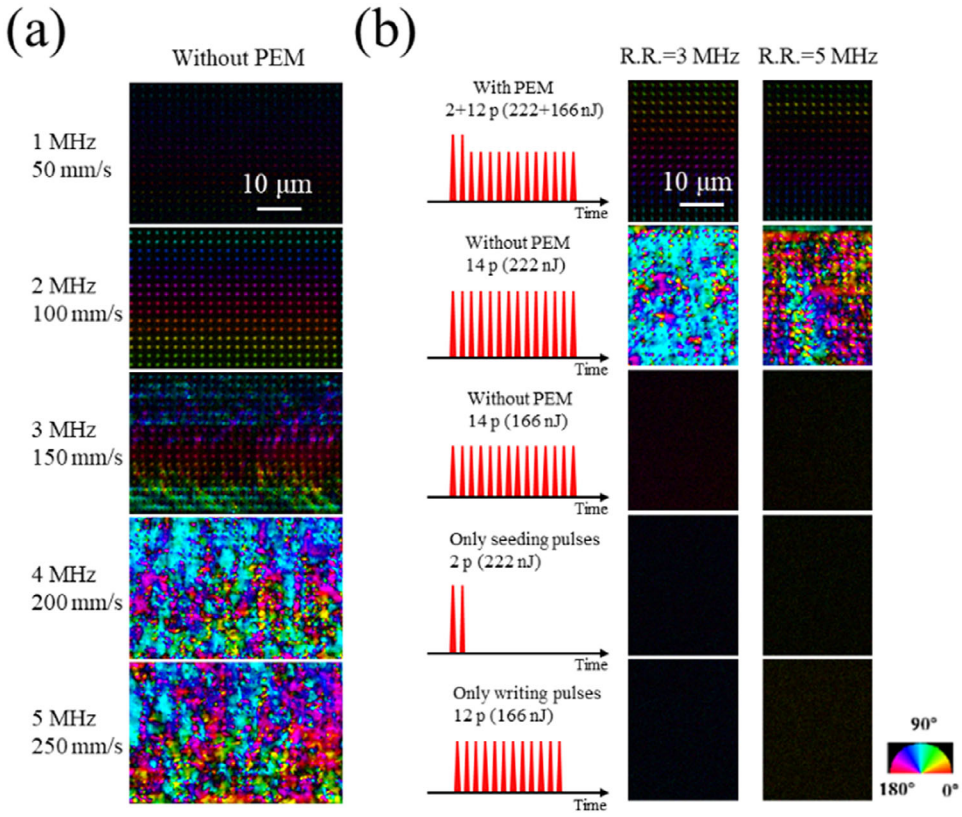

Figure 4. Femtosecond laser direct writing of birefringence structures with and without PEM. a) Images of birefringent voxels written by 15 laser pulses with the energy of 182 nJ at different repetition rates from 1 to 5 MHz. b) Birefringent images of voxels imprinted with and without energy-modulated pulses: 2 seeding pulses and 12 writing pulses (top), 14 pulses with seeding energy (middle top), 14 pulses with writing energy (middle), only 2 seeding pulses (middle bottom), and only 12 writing pulses (bottom). The seeding and writing pulse energies are 222 nJ (212 nJ) and 166 nJ (158 nJ) for repetition rate of 3 MHz (5 MHz). Processing conditions: 650 fs pulse duration, 1030 nm wavelength, 0.3 NA lens.

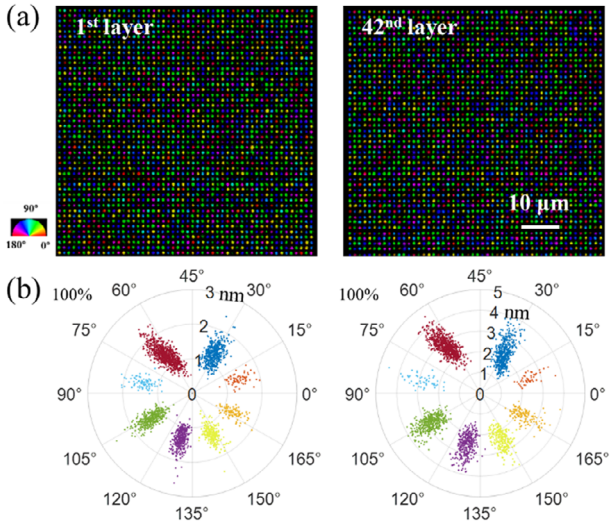

Figure 5. Optical data recording of a digital book with a high writing speed of 72 kB s^{-1}. a) Birefringence images of data voxels of different layers. b) Polar diagram of the measured retardance and azimuth of all voxels in (a). The scanning speed is 250 mm s^{-1} and the lateral voxel separation is 1.3 µm.

3. Conclusion

In conclusion, we demonstrated an increase in the birefringence of nanopore-based modification and positive refractive index change by ultrafast laser writing in silica glass when scanning speed increases. Contrary to intuition, a stronger modification is produced at lower energy density because of the nonlocality of light matter interaction in strongly nonlinear regime, which is confirmed by the observation of the second harmonic generation. In contrast to the nanograting formation regime, we did not observe blue luminescence of self-trapped excitons at 2.8 eV in the regime of nanopore formation. In addition, pulse energy modulation was demonstrated in the regime of nanopore formation enabling high-speed ultrafast laser writing without heat accumulation at high pulse repetition rates. By using a multi-channel experimental setup, it allows one to achieve the writing speed as high as several megabytes per second (MBs^{-1}) with advantages of high transmission and high data accuracy.

4. Experimental Section

Two different laser systems were used to cover a broad range of laser parameters, a mode-locked regeneratively amplified femtosecond (fs) laser

system (PHAROS, Light Conversion Ltd.), operating at a wavelength of 1030 nm with a repetition rate (*RR*) varying from 10 kHz to 1 MHz and a pulse duration (τ) of 300 fs and a Yb-doped fiber fs laser (Satsuma, Amplitude), operating at 1030 nm with a repetition rate from 1 MHz to 10 MHz and a pulse duration tuned in the range of 250–650 fs. The pulse energy modulation was achieved by controlling the electro-optic modulator (EOM) in the fs laser system. The polarization of the writing laser beam was controlled by a combination of a linear polarizer, an electro-optic modulator, and a quarter waveplate. Laser pulses were focused via an aspheric lens with different effective numerical apertures (NA = 0.16, 0.23, or 0.4, Newport) into silica glass sample, which was placed on a three-axial air-bearing translation stage (Aerotech Ltd.).

The retardance and slow axis azimuths of birefringent voxels were quantitatively characterized with a birefringence measurement system (Cri, Abrio imaging system) equipped on the Olympus BX51 optical microscope operating at 546 nm wavelength. The refractive index changes were characterized with a wavefront sensor (SID4-HR, Phasics) mounted on the same microscope.

Supporting Information

Supporting Information is available from the Wiley Online Library or from the author.

Acknowledgements

The study was supported by European Research Council (ENIGMA, 789116), Microsoft (Project Silica) and Horison2020 Marie Curie RISE project #101007896 (CHARTIST). Y.Svirko was grateful to Academy of Finland (Flagship Programme PREIN, decision 34651, and grant 343393) for support. The authors were grateful to Yang Liao from Shanghai Institute of Optics and Fine Mechanics for providing the porous glass.

Conflict of Interest

The authors declare no conflict of interest.

Data Availability Statement

The data that support the findings of this study are available from the corresponding author upon reasonable request.

Keywords

light-matter interaction, nanostructuring in silica glass, optical data storage, ultrafast laser writing

Received: November 6, 2023
Revised: March 11, 2024
Published online:

[1] D. Strickland, G. Mourou, *Opt. Commun.* **1985**, *55*, 447.
[2] S. Backus, C. G. Durfee, M. M. Murnane, H. C. Kapteyn, *Rev. Sci. Instrum.* **1998**, *69*, 1207.
[3] A. C. Tien, S. Backus, H. Kapteyn, M. Murnane, G. Mourou, *Phys. Rev. Lett.* **1999**, *82*, 3883.
[4] A. Vogel, J. Noack, G. Hüttman, G. Paltauf, *Appl. Phys. B* **2005**, *81*, 1015.
[5] P. P. Rajeev, M. Gertsvolf, P. B. Corkum, D. M. Rayner, *Phys. Rev. Lett.* **2009**, *102*, 083001.
[6] D. Grojo, M. Gertsvolf, S. Lei, T. Barillot, D. M. Rayner, P. B. Corkum, *Phys. Rev. B* **2010**, *81*, 212301.
[7] R. Stoian, *Appl. Phys. A* **2020**, *126*, 438.
[8] D. Du, X. Liu, G. Korn, J. Squier, G. Mourou, *Appl. Phys. Lett.* **1994**, *64*, 3071.
[9] B. C. Stuart, M. D. Feit, A. M. Rubenchik, B. W. Shore, M. D. Perry, *Phys. Rev. Lett.* **1995**, *74*, 2248.
[10] P. G. Kazansky, Y. Shimotsuma, M. Sakakura, M. Beresna, M. Gecevičius, Y. Svirko, S. Akturk, J. Qiu, K. Miura, K. Hirao, *Opt. Express* **2011**, *19*, 20657.
[11] K. M. Davis, K. Miura, N. Sugimoto, K. Hirao, *Opt. Lett.* **1996**, *21*, 1729.
[12] J. W. Chan, T. Huser, S. Risbud, D. M. Krol, *Opt. Lett.* **2001**, *26*, 1726.
[13] A. M. Streltsov, N. F. Borrelli, *J. Opt. Soc. Am. B* **2002**, *19*, 2496.
[14] Y. Shimotsuma, P. G. Kazansky, J. Qiu, K. Hirao, *Phys. Rev. Lett.* **2003**, *91*, 247405.
[15] Y. Liao, J. Ni, L. Qiao, M. Huang, Y. Bellouard, K. Sugioka, Y. Cheng, *Optica* **2015**, *2*, 329.
[16] Y. Bellouard, A. Champion, B. McMillen, S. Mukherjee, R. R. Thomson, C. Pépin, P. Gillet, Y. Cheng, *Optica* **2016**, *3*, 1285.
[17] A. Rudenko, J. P. Colombier, T. E. Itina, R. Stoian, *Adv. Opt. Mater.* **2021**, *9*, 2100973.
[18] M. Sakakura, Y. Lei, L. Wang, Y. H. Yu, P. G. Kazansky, *Light Sci. Appl.* **2020**, *9*, 15.
[19] E. N. Glezer, M. Milosavljevic, L. Huang, R. J. Finlay, T.-H. Her, J. P. Callan, E. Mazur, *Opt. Lett.* **1996**, *21*, 2023.
[20] S. Juodkazis, H. Misawa, T. Hashimoto, E. G. Gamaly, B. Luther-Davies, *Appl. Phys. Lett.* **2006**, *88*, 201909.
[21] J. Burghoff, S. Nolte, A. Tünnermann, *Appl. Phys. A* **2007**, *89*, 127.
[22] D. Wei, C. Wang, H. Wang, X. Hu, D. Wei, X. Fang, Y. Zhang, D. Wu, Y. Hu, J. Li, S. Zhu, M. Xiao, *Nat. Photonics* **2018**, *12*, 596.
[23] B. Zhang, D. Tan, Z. Wang, X. Liu, B. Xu, M. Gu, L. Tong, J. Qiu, *Light Sci. Appl.* **2021**, *10*, 93.
[24] K. Sun, D. Tan, X. Fang, X. Xia, D. Lin, J. Song, Y. Lin, Z. Liu, M. Gu, Y. Yue, J. Qiu, *Science* **2022**, *375*, 307.
[25] V. D. Michele, M. Royon, E. Marin, A. Alessi, A. Morana, A. Boukenter, M. Cannas, S. Girard, Y. Ouerdane, *Opt. Mater. Express* **2019**, *9*, 4624.
[26] C. Hnatovsky, R. S. Taylor, P. P. Rajeev, E. Simova, V. R. Bhardwaj, D. M. Rayner, P. B. Corkum, *Appl. Phys. Lett.* **2005**, *87*, 014104.
[27] W. J. Reichman, D. M. Krol, L. Shah, F. Yoshino, A. Arai, S. M. Eaton, P. R. Herman, *J. Appl. Phys.* **2006**, *99*, 123112.
[28] F. Zhang, Y. Yu, C. Cheng, Y. Dai, J. Qiu, *Opt. Lett.* **2013**, *38*, 2212.
[29] S. E. Wei, Y. Wang, H. Yao, M. Cavillon, B. Poumellec, G. D. Peng, M. Lancry, *Sensors* **2020**, *20*, 762.
[30] G. Corrielli, A. Seri, M. Mazzera, R. Osellame, H. de Riedmatten, *Phys. Rev. Appl.* **2016**, *5*, 054013.
[31] C. Hernández-García, A. Turpin, J. S. Román, A. Picón, R. Drevinskas, A. Cerkauskaite, P. G. Kazansky, C. G. Durfee, *I. nigo J. Sola, Optica* **2017**, *4*, 520.
[32] Y. Bellouard, A. Said, M. Dugan, P. Bado, *Opt. Express* **2004**, *12*, 2120.
[33] P. Zijlstra, J. W. Chon, M. Gu, *Nature* **2009**, *459*, 410.
[34] T. Allsop, M. Dubov, V. Mezentsev, I. Bennion, *Appl. Opt.* **2010**, *49*, 1938.
[35] Microsoft Project Silica https://www.microsoft.com/en-us/research/project/project-silica/, (accessed: December 2023).
[36] H. Wang, Y. Lei, L. Wang, M. Sakakura, Y. Yu, G. Shayeganrad, P. G. Kazansky, *Laser Photonics Rev.* **2022**, *16*, 2100563.
[37] Y. Lei, M. Sakakura, L. Wang, Y. Yu, H. Wang, G. Shayeganrad, P. G. Kazansky, *Optica* **2021**, *8*, 1365.
[38] M. K. Bhuyan, M. Somayaji, A. Mermillod-Blondin, F. Bourquard, J. P. Colombier, R. Stoian, *Optica* **2017**, *4*, 951.

[39] J. Zhu, T. M. Horning, M. Zohrabi, W. Park, J. T. Gopinath, *Optica* **2020**, *7*, 1645.
[40] E. M. Dianov, P. G. Kazanskiĭ, D. Y. Stepanov, *Sov. J. Quantum Electron.* **1989**, *19*, 575.
[41] D. Z. Anderson, V. Mizrahi, J. E. Sipe, *Opt. Lett.* **1991**, *16*, 796.
[42] Y. Lei, H. Wang, L. Skuja, B. Kühn, B. Franz, Y. Svirko, P. G. Kazansky, *Laser Photonics Rev.* **2023**, *17*, 2200978.
[43] Y. Lei, G. Shayeganrad, H. Wang, M. Sakakura, Y. Yu, L. Wang, D. Kliukin, L. Skuja, Y. Svirko, P. G. Kazansky, *Light Sci. Appl.* **2023**, *12*, 74.
[44] A. Couairon, L. Sudrie, M. Franco, B. Prade, A. Mysyrowicz, *Phys. Rev. B* **2005**, *71*, 125435.
[45] P. Audebert, P. Daguzan, A. Dos Santos, J. C. Gauthier, J. P. Geindre, S. Guizard, G. Hamoniaux, K. Krastev, P. Martin, G. Petite, A. Antonetti, *Phys. Rev. Lett.* **1994**, *73*, 1990.
[46] P. Martin, S. Guizard, P. Daguzan, G. Petite, P. D'oliveira, P. Meynadier, M. Perdrix, *Phys. Rev. B* **1997**, *55*, 5799.
[47] R. R. Gattass, E. Mazur, *Nat. Photonics* **2008**, *2*, 219.
[48] P. F. Kashaykin, A. L. Tomashuk, M. Y. Salgansky, A. N. Guryanov, E. M. Dianov, *J. Appl. Phys.* **2017**, *121*, 213104.
[49] K. Dholakia, N. Simpson, M. Padgett, L. Allen, *Phys. Rev. A* **1996**, *54*, R3742.
[50] A. Bahabad, A. Arie, *Opt. Express* **2007**, *15*, 17619.
[51] M. Beresna, P. G. Kazansky, Y. Svirko, M. Barkauskas, R. Danielius, *Appl. Phys. Lett.* **2009**, *95*, 121502.
[52] G. Papon, N. Marquestaut, Y. Petit, A. Royon, M. Dussauze, V. Rodriguez, T. Cardinal, L. Canioni, *J. Appl. Phys.* **2014**, *115*, 113103.
[53] P. N. Saeta, B. I. Greene, *Phys. Rev. Lett.* **1993**, *70*, 3588.
[54] D. G. Papazoglou, S. Tzortzakis, *Opt. Mater. Express* **2011**, *1*, 625.
[55] C. Corbari, A. Champion, M. Gecevičius, M. Beresna, Y. Bellouard, P. G. Kazansky, *Opt. Express* **2013**, *21*, 3946.